# Threading the Spindle: A Geometric Study of Chiral Liquid Crystal Polymer Microparticles

Helen S. Ansell, Dae Seok Kim, Randall D. Kamien, Eleni Katifori, and Teresa Lopez-Leon

Phys. Rev. Lett. **123**, 157801 — Published 10 October 2019

DOI: 10.1103/PhysRevLett.123.157801

# Threading the spindle: a geometric study of chiral liquid crystal polymer microparticles

Helen S. Ansell*,[1] Dae Seok Kim*,[1,2] Randall D. Kamien†,[1] Eleni Katifori,[1] and Teresa Lopez-Leon† [2]

[1] *Department of Physics and Astronomy, University of Pennsylvania, Philadelphia, Pennsylvania 19104, USA*
[2] *UMR CNRS 7083, ESPCI Paris, PSL Research University, 75005 Paris, France*

(Dated: September 13, 2019)

Polymeric particles are strong candidates for designing artificial materials capable of emulating the complex twisting-based functionality observed in biological systems. In this letter, we provide the first detailed investigation of the swelling behavior of bipolar polymer liquid crystalline microparticles. Deswelling from the spherical bipolar configuration causes the microparticle to contract anisotropically and twist in the process, resulting in a twisted spindle shaped structure. We propose a model to describe the observed spiral patterns and twisting behavior.

From the twisting of DNA and proteins to the twirling of plant tendrils and the wringing of a wet towel [1], torsional and twisting motion is an inevitable and common occurrence at all scales. Twisting motion allows many organisms to achieve their complex mechanical functions including swimming [2], flying [3], crawling [4], climbing [5], seedpod opening [6], and energy storage [7], so nature has evolved a broad range of ingenious mechanisms to achieve it. The three-dimensional twisting and torsional actuation of biological systems often originates from anisotropic internal microstructures with local volume variation. For example, cucumber tendrils coil and wind via asymmetric contraction of an internal fiber ribbon of specialized cells [8, 9] and euglenas swim by uniformed sliding and twisting of their cell walls [10–12]. Emulation of these types of highly controlled twisted shape transformations in nature would provide the capacity and incentive to design active materials with specific twisting-based functionality.

Polymeric particles are one of the strongest candidates for usage in a diverse range of applications including drug delivery [13], emulsion stabilization [14], catalysis [15], separation processes [16], and sensors [17]. The shape complexity, size, and internal morphology of the particles are critical for their specific applications. Liquid crystal polymers (LCPs) can be considered as particularly favorable due to the possibility of designing the structure of the polymer network by templating via the nematic director field. Changes in the shape and structure of the particles, including the emergence of chirality from an initially achiral state, can be driven by changes in external stimuli including heat [18], pH [19], light [20], electric field [21], magnetic field [22], and solvents [23].

LCP microparticles formed from bipolar nematic droplets provide an example of how an initially achiral configuration can lead to a chiral final configuration. Volume contraction, driven by the removal of non-reactive mesogens from the polymeric particles, causes the spherical microparticle to contract anisotropically and twist in the process, resulting in a twisted spindle shaped structure [24, 25]. The mechanism through which the twisting occurs as well as the role of the bipolar configuration and the interplay between geometric frustration and bulk instabilities in initially curved droplets remain poorly understood. In this letter, we report the first detailed investigation into the behavior of these twisted particles. By carefully controlling the swelling of the microparticles using a binary solvent mixture [23], we are able to stabilize the intermediate states between the initial, achiral spherical structure and the final, twisted, spindle structure and measure the relationship between the aspect ratio of the microparticle $u$ and twist angle of the polymer strands at the surface $\beta$. We find that the microparticles deswell following a two-step process: below a critical $u$ value, they shrink predominantly by inner folding of the polymer bundles, while above the critical value, they shrink mostly by twisting. We show that the particles twist from the surface inwards by aligning their polymer strands along loxodromes, or lines of constant bearing. We propose a model to describe the observed spiral patterns and twisting behavior. Our results suggests a strategy to design chiral spindle-shaped particles with tunable twist in addition to possible sensing or actuation capabilities.

We used microfluidics to fabricate polymeric microliquid crystal (LC) droplets with diameters of approximately 100 $\mu$m using a three-component polymerizable mixture of 4-cyano-4′-pentylbiphenyl (5CB, Merck), reactive LC monomer 4-(3-acryloyoxy-propyloxy) benzoic acid 2-methyl-1,4-phenylene ester (RM257), and 2wt% of photoinitiator (Irgacure 369, Ciba) with respect to the amount of RM257, dispersed in aqueous solution containing 1wt% polyvinyl alcohol (PVA) [26]. PVA stabilizes the droplets and enforces planar anchoring at the interface between the liquid crystal and aqueous solution. For most liquid crystals, this type of boundary condition results in the formation of a bipolar configuration, schematically represented in FIG. 1(a) (left) [27], where the molecules align in average along the meridians of the sphere, producing two surface defects, or boojums, at the points where the meridians intercept.

When UV light is shone on the droplets, the RM257

polymerizes in an end-to-end configuration. After polymerization of the RM257, the polymeric particles show preservation of the bipolar configuration, indicating that the majority of RM257 is well oriented along the director field of non-reactive monomers prior to polymerization and that this alignment is preserved during the polymerization process [25, 28]. The bipolar configuration is shown in the polarized optical microscopy (POM) images of the particles after polymerization (FIG. 1(b-c)) as well as in the surface topography shown in the scanning electron microscopy (SEM) image in FIG. 1(d). Subsequent extraction of the 5CB from the polymeric droplets using ethanol results in pronounced shrinkage of the microparticles in all directions, but with greater shrinking along the directions perpendicular to the line connecting the two boojums. The resulting polymer particles therefore adopt a spindle shape with the defects at the tips, as shown in the schematic in FIG. 1(a) (right). During the deswelling process, the particles also adopt a twisted pattern as they shrink, as shown in the bottom row of FIG. 1 and in MOV. S1 of the supplementary material. We note that by repeating the same procedure with the droplet in the isotropic phase (approx. 50°C with 5 wt% RM257), the resulting polymer network is randomly oriented. Upon removal of the 5CB the remaining polymer particle crumples, as shown in FIG. 1(e), demonstrating the importance of the initial design of the polymer network in its structure and function.

When the amount of RM257 is below 20 wt% we almost always observe twisted spindle structures (see supplementary information). Conversely, if the proportion of RM257 in the initial LC state is too high, the reduction in volume of the resulting particle during shrinking is much smaller and the twisting pattern is not observed, as shown in FIG. S2 of the supplementary material for a preparation with 40 wt% RM257. The higher density of the polymer network means that the polymer bundles are closer to each other in the initial configuration. Removing the 5CB creates less free space within the polymer particle into which the polymer can move. Volume reduction through twisting therefore is not preferable in this case. Thus, here, we report and characterize the twisting behavior for 5 wt% and 20 wt% of RM257.

We produced equilibrium polymer structures using a mixture of chloroform and ethanol, in which chloroform and ethanol are the swelling and deswelling solvents for poly(RM257), respectively, and studied the relationship between the twist angle $\beta$ and aspect ratio $u$. Experimentally, we measure $\beta$ as the angle between the meridian connecting the poles of the particle and the lines of the polymer texture at the equator. As $\chi_{\mathrm{EtOH}}$ increases, $u$ and $\beta$ both increase, as shown in FIG. 2(a), with the growth rate higher for 5 wt% RM257 than for 20 wt%.

By plotting the values of $\beta$ and $u$ on a single graph, as shown in FIG. 2(b), we observe that the data for the two different initial polymer densities appear to fall on

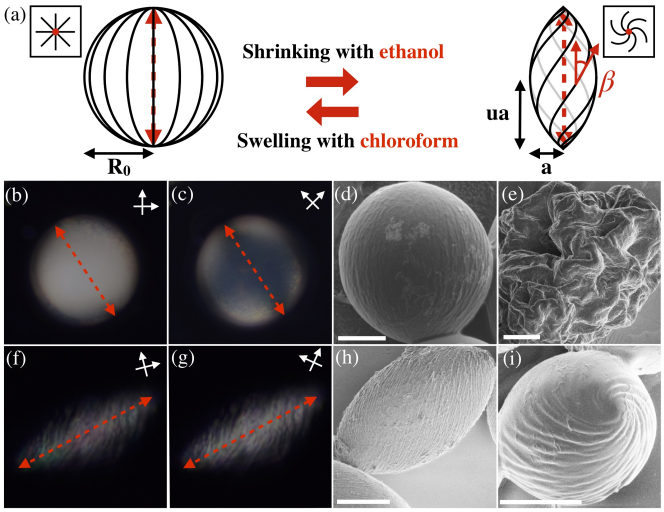


FIG. 1. (a) Schematic of shrinking and swelling process. The square insets on the top left and top right indicate a top view of the director field at the boojums. (b)-(d) Spherical polymer particle after polymerization and before removal of 5CB. (b)-(c) POM images of particles showing that they are in the bipolar configuration: there is light extinction only when the line connecting the two boojums (optical axis) is aligned with the analyzer/polarizer. (d) SEM image of bipolar configuration. (e) SEM image of crumpling if polymerization takes place in the isotropic phase. (f)-(i) Twisted spindle particle after shrinking. (f)-(g) POM images: there is no complete light extinction at any angle when rotating the sample, indicating that the twist angle changes through the particle. (h) SEM side view. (i) SEM top view. All scale bars are 20 $\mu$m. Dashed red arrows on POM images indicate the axis connecting the two boojums.

a single curve and that the twisting process shows two distinct stages, as illustrated in FIG. 3(a-d) that show polymer particles at different stages of dewelling. Initially, the polymer particles are approximately spherical and show no twisting, as is shown in FIG. 3(a) for a particle with $u = 1.1$ and $\beta = 0°$. The particles then start to deswell anisotropically into spindle shapes, as in FIG. 3(b) ($u = 1.28$, $\beta = 7°$). This initial deswelling, in the region for $u < 1.36$, shows a small increase in $\beta$ as $u$ increases. However, for $u > 1.36$, there is a sharp increase in $\beta$ with respect to $u$ before the behavior slows at larger $u$. FIG. 3(c) shows a spindle with $u = 1.43$ and $\beta = 19°$, which corresponds to the region of sharp increase of $\beta$ with $u$, while FIG 3(d) shows a fully deswelled particle with $u = 2.34$ and $\beta = 46°$.

In order to understand the observed behavior, we first consider the shape of the particles as they deswell. In the initial spherical state, the nematic director field lines in the bulk follow the edges of concentric spindles with decreasing minor axis from the surface to the center of the droplet, and the two defects [29] sit at the tips. Prior work predicts that for bipolar nematic droplets, a spindle shape minimizes the free energy regardless of the elastic

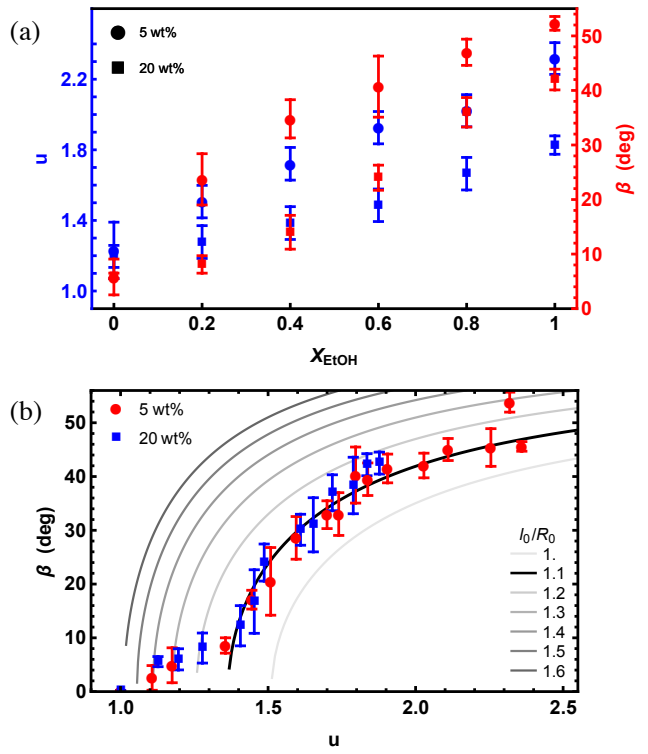


FIG. 2. (a) Experimental data for how aspect ratio $u$ and twist angle $\beta$ vary with fractional concentration of ethanol $\chi_{EtOH}$. (b) Experimental data and loxodrome model for twist angle as a function of aspect ratio.

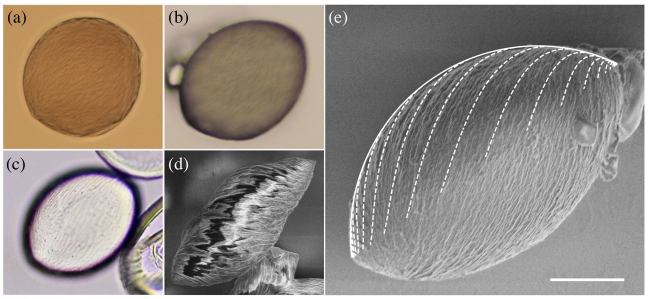


FIG. 3. (a)-(d) Images of polymer microparticles at different stages of deswelling. (a) OM with $u = 1.1$, $\beta = 0°$, (b) OM with $u = 1.28$, $\beta = 7°$, (c) OM with $u = 1.43$, $\beta = 19°$, (d) SEM with $u = 2.34$, $\beta = 46°$. (e) SEM image of a polymer particle with $u = 1.7$ and $\beta = 33°$. The spindle loxodrome model is plotted over half of the image. The solid white line indicates the spindle outline while the dashed lines show the loxodrome spirals as they would appear on the surface. The scale bar is 10 $\mu$m.

constants [30], consistent with our observation of a spindle shape.

A spindle is formed as the surface of revolution of the minor arc of a circle about the chord connecting its endpoints. We describe our spindles of semi-minor axis length $a$ and aspect ratio $u \geq 1$ using cylindrical coordinates $(r, \theta, z)$, where the spindle major axis is parallel to the $\hat{\mathbf{z}}$ direction. The radius of the spindle varies from $r = 0$ at $z = \pm ua$ to $r = a$ at $z = 0$. A position on the surface is described by the vector $\mathbf{r} = (r\cos\theta, r\sin\theta, z(r))$, where the height $z(r) = \pm a\sqrt{(1 - r/a)\,(u^2 + r/a)}$.

There are two distinct mechanisms by which the polymer particle volume can change as the solvent composition is varied. One is a change in the effective length of the polymer chains due to interactions with the solvents. The other is for the polymers to maintain a fixed effective length and rearrange to reduce the overall particle volume. We will demonstrate that our results are consistent with both of these mechanisms contributing to the formation of the twisted spindles.

We now consider a twisting mechanism for fixed polymer chain length, considering explicitly only the twisting pattern on the surface. Note, however, that the mechanism presented also applies to each layer within the bulk, resulting in a structure in which the twist angle increases from zero at the center of the particle to a maximum value on the surface [31]. Theoretical studies demonstrate that twisted configurations are stable in bipolar nematic droplets if the bend and twist elastic constants are small enough in comparison to the splay elastic constant [31, 32].

In order for a particle to reduce in volume, the surface area of each layer must reduce. If the polymer chains within a layer have a fixed length, chains which were initially meridians (lines of longitude) are too long to fit as meridians on the smaller surface below. The chains must therefore rotate in order to accommodate their excess length, resulting in an elongated twisted structure. To accurately describe the twisting pattern, we take additional measurements of the twist angle at different points on the surface, transforming measured angles into angles relative to the surface meridians, as demonstrated in FIG. S3 of the supplementary information. Our results indicate that the twist angle relative to the local meridian is independent of position on the surface. A curve of this type, for which the tangent vector is always at the same fixed angle with respect to the local meridian, is referred to as a *loxodrome*, a term used in navigation to describe a course of constant bearing [33].

That loxodromes are the integral curves of the director field on the surface of a twisted-spindle shaped nematic structure has been previously assumed in theoretical studies that consider the bulk structure of twisted bipolar tactoids [31, 32]. Why should this be? The solvents used for swelling and deswelling are not mesogenic but are isotropic. Thus if the response of the RM257 is dominated by solvent effects then we expect tilting that is independent of position – a constant angle loxodrome. Moreover, we also note that templating two dimensional nematic elastomers with a director field for which the integral curves are logarithmic spirals results in the formation of a conical structure [34]. After activation, these

curves trace out loxodromes on the conical surface. Thus, the loxodrome model also predicts that the tips of the spindle are conical and not blunted – consistent with our observations of pointed, conical tips on the spindle rather than an ellipsoid. As we will see, the loxodrome model also can be used to rationalize the angle versus aspect ratio data in FIG. 2.

A loxodrome of twist angle $\beta$, defined as the angle between the meridian and the curve (see schematic in FIG. 1(a)), must have its tangent vector parallel to the unit vector $\hat{\beta} = \cos\beta\,\hat{\mathbf{e}}_v + \sin\beta\,\hat{\mathbf{e}}_\theta$ , where $\hat{\mathbf{e}}_v = (\cos\theta, \sin\theta, z')/\sqrt{1+z'^2}$ and $\hat{\mathbf{e}}_\theta = (-\sin\theta, \cos\theta, 0)$ are orthonormal vectors on the surface, and prime notation indicates a derivative with respect to $r$. To satisfy this requirement on the spindle, the curve $\theta_c(r)$ must obey

$$\frac{\mathrm{d}\theta_c}{\mathrm{d}r} = \frac{\left(1+u^2\right)\tan\beta}{2r\sqrt{(1-r/a)\,(u^2+r/a)}}. \tag{1}$$

Solving for $\theta_c(r)$ and choosing $\theta_c(a) = 0$ as the integration constant leads to the equation of the spindle loxodrome:

$$\theta_c(r) = (u+u^{-1})\tan\beta\tanh^{-1}\left[\frac{(1-r/a)u^2}{u^2+r/a}\right]^{1/2}. \tag{2}$$

We consider polymer chains along the surface of the particle extending from the spindle tip to the equator. If these surface strands have fixed length $l_0$, the twist angle $\beta$ as a function of $a$ and $u$ can be determined from EQ. (2):

$$\beta = \cos^{-1}\left[\frac{a}{l_0}\left(1+u^2\right)\tan^{-1}\left(u^{-1}\right)\right]. \tag{3}$$

Experimentally, we observe a linear relationship between the change in major and minor axis length during dewelling (see supplementary FIG. S4), leading to the relation

$$u = 0.54R_0/a + 0.48, \tag{4}$$

where $R_0$ is the initial radius of the polymer particle ($\sim 50\,\mu m$). Using this relationship, we can write $\beta$ (EQ. (3)) in terms of the single variable $u$ for fixed $l_0$.

During deswelling the final major axis length of the particles is determined by bulk properties, specifically the decrease in length of a polymer chain directly through the center of the particle connecting the two boojums. Experimentally, we observe a 30% reduction in length of the major axis. A polymer strand along an initially spherical particle from a pole to the equator has length $\pi R_0/2 \approx 1.6R_0$. Assuming that all polymer strands reduce in length by the same 30%, we expect the surface strand will have a final length of $1.1R_0$ in the twisted state, corresponding to a length of $\sim 55\ \mu m$. We therefore use this value as the length $l_0$ of the polymer strands on the surface. Put together, we plot $\beta$ as a function of $u$ for different values of $l_0/R_0$. There is good agreement between the model and experimental results for the curve with $l_0 = 1.1R_0$ for $u > 1.36$, consistent with the prediction that the twisting mechanism dominates in this region and that the surface chains have a final length $l_0 = 1.1R_0$. FIG. 3(e) shows an SEM image with the spindle outline and loxodrome curves superimposed over half of the image to demonstrate how the model compares with the data.

What about for $u \leq 1.36$? The twisting mechanism dominates the volume reduction *after* the length of a meridian from the pole to the equator of the spindle shrinks to $1.1R_0$. Using (4) to find the value of $u$ when $\beta = 0$ we find that the meridian of the spindle reaches this length when $u \approx 1.36$. For $1 < u < 1.36$, the twist angle varies slowly with aspect ratio and increases from zero to ten degrees in this range. This is a much slower rate of increase of angle than is observed for $u$ slightly larger than the transition value, where the twisting mechanism dominates. In this regime, the volume decrease is dominated by polymer folding, consistent with the data points crossing curves on the graph in FIG. 3(b) for larger values of $l_0$ than the final value $l_0 = 1.1R_0$. There is some twisting observed in this region due to it still providing a mechanism through which the polymer particle can lose volume.

Note that the surface polymer reaches its final length partway through the deswelling process and that the major and minor axes change continuously throughout deswelling, suggesting that the particles shrink from the surface inwards. While strands at the center do not reach their minimum length until $\chi_{EtOH}$ is maximal, strands near the surface reach their final length earlier in the shrinking process.

Finally, we would like to highlight that the shrinking and twisting mechanisms described above are fully reversible, providing interesting possibilities for applications. During ten repeated swelling and deswelling cycles (swelling in chloroform from the twisted state to $u = 1.1$; dewswelling in pure ethanol to $u = 1.8$ for 20 wt% RM257) the particles showed complete reversibility. This suggests that the polymer particles could be used for long-term actuating capability and reliability. While it is possible to swell the particles until they are almost perfectly spherical, it is not possible to change the chirality of the twisting through the swelling process. That is, while there is an equal likelihood of a given particle having either handedness, once a particle has twisted in a given direction it will always twist in that direction even after swelling back to almost spherical and shrinking again. This indicates that although the bipolar configuration itself is achiral, there must be fluctuations within the nematic droplets during the preparation process that dictate the chirality of the twisting that gets locked in through polymerization.

Since $\beta$ and $u$ are highly controllable with solvents, these values could be carefully calibrated against the fractional concentration of any binary solvent mixture in which one solvent causes swelling of the polymer particles and the other causes shrinking. The particles could then be used as a quickly responsive and quantitative indicator of the fractional concentration of solvents in the mixture. With further efforts to assemble those twisted particles into three dimensional forms, they may be used as a template in the fabrication of complex three dimensional helical structures for metastable opto-electric devices [35, 36]. Our one-pot production of chiral spindles may also be the basis for the study of the isotropic-nematic (or isotropic-cholesteric) transition as a function of aspect ratio at fixed concentration, providing a novel variable for probing Onsager's seminal result [37].

The authors would like to thank K. Dalnoki-Veress and E. Raphaël for fruitful discussions. HSA, DSK, and RDK were supported by NSF MRSEC Grant DMR-1720530 and a Simons Investigator Grant from the Simons Foundation to RDK. TLL and DSK were supported by the French National Research Agency Grant 13-JS08-0006-01. EK acknowledges support by NSF MRSEC Grant DMR-1720530, the NSF Award PHY-1554887, and the Simons Foundation. R.D.K. and H.S.A. would like to thank the Isaac Newton Institute for Mathematical Sciences for support and hospitality during the programme The Mathematical Design of New Materials when work on this paper was undertaken. This work was also supported by EPSRC Grant Number EP/R014604/1.

* These authors contributed equally to this work.

† Corresponding authors.

[1] H. D. Rahmayanti, F. D. Utami, and M. Abdullah, European Journal of Physics **37**, 065806 (2016).
[2] M. Arroyo, L. Heltai, D. Millán, and A. DeSimone, Proceedings of the National Academy of Sciences of the United States of America **109**, 17874 (2012).
[3] J. Young, S. M. Walker, R. J. Bomphrey, G. K. Taylor, and A. L. R. Thomas, Science **325**, 1549 (2009).
[4] H. Marvi, C. Gong, N. Gravish, H. Astley, M. Travers, R. L. Hatton, J. R. Mendelson, H. Choset, D. L. Hu, and D. I. Goldman, Science **346**, 224 (2014).
[5] S. Isnard and W. K. Silk, American Journal of Botany **96**, 1205 (2009).
[6] Y. Forterre and J. Dumais, Science **333**, 1715 (2011).
[7] L. Mahadevan and P. Matsudaira, Science **288**, 95 (2000).
[8] S. J. Gerbode, J. R. Puzey, A. G. McCormick, and L. Mahadevan, Science **337**, 1087 (2012).
[9] J.-S. Wang, G. Wang, X.-Q. Feng, T. Kitamura, Y.-L. Kang, S.-W. Yu, and Q.-H. Qin, Scientific Reports **3**, 3102 (2013).
[10] G. Noselli, M. Arroyo, and A. DeSimone, Journal of the Mechanics and Physics of Solids **123**, 234 (2019).
[11] G. Noselli, A. Beran, M. Arroyo, and A. DeSimone, Nature Physics **15**, 496 (2019).
[12] M. Arroyo and A. DeSimone, Journal of the Mechanics and Physics of Solids **62**, 99 (2014).
[13] K. J. Pekarek, J. S. Jacob, and E. Mathiowitz, Nature **367**, 258 (1994).
[14] B. Madivala, S. Vandebril, J. Fransaer, and J. Vermant, Soft Matter **5**, 1717 (2009).
[15] C. Cui, L. Gan, M. Heggen, S. Rudi, and P. Strasser, Nature Materials **12**, 765 (2013).
[16] M. E. Davis, Nature **417**, 813 (2002).
[17] B. Gider, P. S. Ghosh, C.-C. You, S. A. Krovi, I.-B. Kim, B. Erdogan, O. R. Miranda, V. M. Rotello, and U. H. F. Bunz, Nature Nanotechnology **2**, 318 (2007).
[18] T. H. Ware, M. E. McConney, J. J. Wie, V. P. Tondiglia, and T. J. White, Science **347**, 982 (2015).
[19] D. Klinger, C. X. Wang, L. A. Connal, D. J. Audus, S. G. Jang, S. Kraemer, K. L. Killops, G. H. Fredrickson, E. J. Kramer, and C. J. Hawker, Angewandte Chemie International Edition **53**, 7018 (2014).
[20] C. L. van Oosten, C. W. M. Bastiaansen, and D. J. D. Broer, Nature Materials **8**, 677 (2009).
[21] E. W. H. Jager, E. Smela, and O. Inganäs, Science **290**, 1540 (2000).
[22] R. Tang, Z. Liu, D. Xu, J. Liu, L. Yu, and H. Yu, ACS Applied Materials and Interfaces **7**, 8393 (2015).
[23] T. Kamal and S.-Y. Park, Chemical Communications **50**, 2030 (2014).
[24] J.-H. Lee, T. Kamal, S. V. Roth, P. Zhang, and S.-Y. Park, RSC Advances **4**, 40617 (2014).
[25] X. Wang, E. Bukusoglu, D. S. Miller, M. A. Bedolla Pantoja, J. Xiang, O. D. Lavrentovich, and N. L. Abbott, Advanced Functional Materials **26**, 7343 (2016).
[26] S.-H. Kim, J. W. Kim, J.-C. Cho, and D. A. Weitz, Lab Chip **11**, 3162 (2011).
[27] P. S. Drzaic, *Liquid Crystal Dispersions* (World Scientific, 1995).
[28] F. Mondiot, X. Wang, J. J. de Pablo, and N. L. Abbott, Journal of the American Chemical Society **135**, 9972 (2013).
[29] R. D. Williams, Rutherford Appleton Laboratory Report No. RAL-85-028 (1985), unpublished.
[30] P. Prinsen and P. van der Schoot, Phys. Rev. E **68**, 021701 (2003).
[31] R. D. Williams, Journal of Physics A: Mathematical and General **19**, 3211 (1986).
[32] P. Prinsen and P. van der Schoot, Journal of Physics: Condensed Matter **16**, 8835 (2004).
[33] K. C. Carlton-Wippern, Journal of Navigation **45**, 292 (1992).
[34] C. D. Modes, K. Bhattacharya, and M. Warner, Proc. R. Soc. A **467**, 1121 (2011).
[35] J. K. Gansel, M. Thiel, M. S. Rill, M. Decker, K. Bade, V. Saile, G. von Freymann, S. Linden, and M. Wegener, Science **325**, 1513 (2009).
[36] N. Yu and F. Capasso, Nature Materials **13**, 139 (2014).
[37] L. Onsager, Annals of the New York Academy of Sciences **51**, 627 (1949).